

A TOTAL ABSORPTION SPECTROMETER FOR GAMMA RAYS

---

MALVERN H. L. JESTER

Library  
U. S. Naval Postgraduate School  
Monterey, California









A TOTAL ABSORPTION SPECTROMETER FOR GAMMA RAYS

\* \* \* \* \*

Malvern H. L. Jester

A TOTAL ABSORPTION SPECTROSCOPY FOR GAMMA RAYS

\*\*\*\*\*

Received 11. 11. 1957



A TOTAL ABSORPTION SPECTROMETER FOR GAMMA RAYS

by

Malvern H. L. Jester  
Lieutenant, United States Navy

Submitted in partial fulfillment  
of the requirements  
for the degree of  
MASTER OF SCIENCE  
in  
PHYSICS

United States Naval Postgraduate School  
Monterey, California

1 9 5 5

A TOTAL ASSASSINATION EFFECTIVE FOR 1947

This  
J478

ALLIANCE OF I. U. S. A.  
LITHOGRAPH, LITHO PRESS, NEW YORK

RESEARCH IN SOCIAL SCIENCE  
IN THE U. S. A.  
FOR THE U. S. A.  
LITHOGRAPH OF SCIENCE  
IN  
NEW YORK

RESEARCH IN SOCIAL SCIENCE  
LITHOGRAPH, LITHO PRESS, NEW YORK

1947

Library  
U. S. Naval Postgraduate School  
Monterey, California

This work is accepted as fulfilling  
the thesis requirements for the degree of

MASTER OF SCIENCE

IN

PHYSICS

from the

United States Naval Postgraduate School



# A TOTAL ABSORPTION SPECTROMETER FOR GAMMA RAYS

Malvern H. L. Jester

Radiation Laboratory  
University of California, Berkeley, California

May 13, 1955

## ABSTRACT

A description of a total-absorption spectrometer for gamma rays is given. The spectrometer depends on the Cherenkov radiation emitted in 14 inches of lead glass by the shower electron-positron pairs formed by an incident gamma ray. The Cherenkov radiation is detected only when four photomultipliers looking at the glass operate in coincidence. The added output of the photomultipliers is analyzed with a ten-channel pulse-height analyzer. The relative pulse-height output of the spectrometer varies linearly as the energy of incident monoenergetic electrons is varied from 42 Mev to 319 Mev. The energy resolution is about 30%. It is believed that the useful range of the spectrometer will extend to several Bev.



## PREFACE

In 1900 it was observed that electroscopes were inexplicably discharged although no known charged body or ionizing agent was near. It is now known that the discharge is partially caused by what later came to be called cosmic rays. Cosmic rays were first studied by Hess (1) in balloon flights in 1912, but were not generally accepted as of extra-terrestrial origin until 1926 (2). Through experiments with the penetration of lead by the rays causing this discharge it became evident that they were of very high energy. When Lawrence (3) invented the cyclotron in 1930 the way was opened for the artificial production of high-energy radiation. Today, with the Bevatron, we can accelerate particles whose energies are equal to those of low-energy cosmic rays.

Gamma rays and electrons, both components of cosmic rays, are also produced in several types of accelerators either directly or indirectly through the bombardment of a target with some other particle such as a proton. Much about the energy of these gamma rays and electrons is still unknown, especially in the higher-energy regions of several billion electron volts. It is believed that the total-absorption spectrometer for electrons and gamma rays described herein will prove useful in analyzing particles in the energy range of several Bev.

The author wishes to acknowledge the guidance of Professor Burton J. Moyer of the Radiation Laboratory at the University of California, Berkeley. He is especially grateful to Dr. Roger Wallace for his guidance, aid, and criticism of this paper. The assistance and advice of John Brabant have been invaluable. The author also wishes to thank Robert Cence, the crews of the synchrotron and Bevatron, and the shop personnel. Finally the author wishes to thank Professor Satosi Watanabe of the United States Naval Post Graduate School, Monterey, California, who reviewed the completed paper.







# TABLE OF CONTENTS

Item	Title	Page
Abstract	. . . . .	ii
Preface	. . . . .	iii
List of Illustrations	. . . . .	v
Table of Symbols and Abbreviations	. . . . .	vi
Chapter I	Introduction . . . . .	1
Chapter II	Theory . . . . .	4
Chapter III	Phototubes . . . . .	9
Chapter IV	Experimental Equipment . . . . .	11
Chapter V	Experiment and Results . . . . .	15
Table I	Glass Characteristics . . . . .	36
Bibliography	. . . . .	37



# LIST OF ILLUSTRATIONS

Figure		Page
1.	Cherenkov Radiation. Huygens construction of wave front. Charged particle moving in positive $x$ direction at velocity $v = \beta c$ . Time required for particle to move from $-4$ cm to $0$ ; $\tau = 4/\beta c$ . In time $\tau = 4/\beta c$ light travels $r = (c/n) \tau = 4/\beta n$ cm. Therefore wavelet starting when particle was at $-4$ cm has radius $4/\beta n$ when particle reaches $0$ . Wavelets reinforce along conical wave front propagated in direction $\theta$ relative to moving particle. $\cos \theta = (4/\beta n)/4 = 1/\beta n$ . . . . .	.20
2.	Graph of the minimum energy of electrons for Cherenkov radiation versus index of refraction. . . . .	.21
3.	Photomultiplier circuits. . . . .	.22
4.	Component parts of the total-absorption gamma-ray spectrometer. . . . .	.23
5.	Calibration layout for the spectrometer at the UCRL synchrotron . . . . .	.24
6.	Electronic arrangement . . . . .	.25
7.	Histogram of cosmic rays observed at the rate of 9.4 counts per second. . . . .	.26
8.	Histogram of the relative pulse-height distribution of 42-Mev and 209-Mev electrons. . . . .	.27
9.	Histogram of the relative pulse-height distribution of 94-Mev electrons. . . . .	.28
10.	Histogram of the relative pulse-height distribution of 119-Mev electrons. . . . .	.29
11.	Histogram of the relative pulse-height distribution of 167-Mev electrons . . . . .	.30
12.	Histogram of the relative pulse-height distribution of 228-Mev electrons. . . . .	.31
13.	Histogram of the relative pulse-height distribution of 251-Mev electrons. . . . .	.32
14.	Histogram of the relative pulse-height distribution of 319-Mev electrons . . . . .	.33
15.	Graph from which the resolution of the spectrometer may be determined . . . . .	.34
16.	Graph of the linear response of the spectrometer from 42 Mev to 319 Mev . . . . .	.35

Page	Topic
1	General Introduction: Background and Objectives of the Conference
2	Summary of the Proceedings: Key Findings and Conclusions
3	Technical Session: Advances in the Field of Research
4	Workshop: Practical Applications of the Research
5	Discussion: Implications for Future Research and Policy
6	Concluding Remarks: The Role of the Conference in the Field
7	References: Bibliography of the Conference Papers
8	Appendix: Additional Information and Data
9	Index: Subject Index and Author Index
10	Table of Contents: Detailed Table of Contents
11	Table of Contents: Detailed Table of Contents
12	Table of Contents: Detailed Table of Contents
13	Table of Contents: Detailed Table of Contents
14	Table of Contents: Detailed Table of Contents
15	Table of Contents: Detailed Table of Contents
16	Table of Contents: Detailed Table of Contents
17	Table of Contents: Detailed Table of Contents
18	Table of Contents: Detailed Table of Contents
19	Table of Contents: Detailed Table of Contents
20	Table of Contents: Detailed Table of Contents
21	Table of Contents: Detailed Table of Contents
22	Table of Contents: Detailed Table of Contents
23	Table of Contents: Detailed Table of Contents
24	Table of Contents: Detailed Table of Contents
25	Table of Contents: Detailed Table of Contents
26	Table of Contents: Detailed Table of Contents
27	Table of Contents: Detailed Table of Contents
28	Table of Contents: Detailed Table of Contents
29	Table of Contents: Detailed Table of Contents
30	Table of Contents: Detailed Table of Contents
31	Table of Contents: Detailed Table of Contents
32	Table of Contents: Detailed Table of Contents
33	Table of Contents: Detailed Table of Contents
34	Table of Contents: Detailed Table of Contents
35	Table of Contents: Detailed Table of Contents
36	Table of Contents: Detailed Table of Contents
37	Table of Contents: Detailed Table of Contents
38	Table of Contents: Detailed Table of Contents
39	Table of Contents: Detailed Table of Contents
40	Table of Contents: Detailed Table of Contents
41	Table of Contents: Detailed Table of Contents
42	Table of Contents: Detailed Table of Contents
43	Table of Contents: Detailed Table of Contents
44	Table of Contents: Detailed Table of Contents
45	Table of Contents: Detailed Table of Contents
46	Table of Contents: Detailed Table of Contents
47	Table of Contents: Detailed Table of Contents
48	Table of Contents: Detailed Table of Contents
49	Table of Contents: Detailed Table of Contents
50	Table of Contents: Detailed Table of Contents
51	Table of Contents: Detailed Table of Contents
52	Table of Contents: Detailed Table of Contents
53	Table of Contents: Detailed Table of Contents
54	Table of Contents: Detailed Table of Contents
55	Table of Contents: Detailed Table of Contents
56	Table of Contents: Detailed Table of Contents
57	Table of Contents: Detailed Table of Contents
58	Table of Contents: Detailed Table of Contents
59	Table of Contents: Detailed Table of Contents
60	Table of Contents: Detailed Table of Contents
61	Table of Contents: Detailed Table of Contents
62	Table of Contents: Detailed Table of Contents
63	Table of Contents: Detailed Table of Contents
64	Table of Contents: Detailed Table of Contents
65	Table of Contents: Detailed Table of Contents
66	Table of Contents: Detailed Table of Contents
67	Table of Contents: Detailed Table of Contents
68	Table of Contents: Detailed Table of Contents
69	Table of Contents: Detailed Table of Contents
70	Table of Contents: Detailed Table of Contents
71	Table of Contents: Detailed Table of Contents
72	Table of Contents: Detailed Table of Contents
73	Table of Contents: Detailed Table of Contents
74	Table of Contents: Detailed Table of Contents
75	Table of Contents: Detailed Table of Contents
76	Table of Contents: Detailed Table of Contents
77	Table of Contents: Detailed Table of Contents
78	Table of Contents: Detailed Table of Contents
79	Table of Contents: Detailed Table of Contents
80	Table of Contents: Detailed Table of Contents
81	Table of Contents: Detailed Table of Contents
82	Table of Contents: Detailed Table of Contents
83	Table of Contents: Detailed Table of Contents
84	Table of Contents: Detailed Table of Contents
85	Table of Contents: Detailed Table of Contents
86	Table of Contents: Detailed Table of Contents
87	Table of Contents: Detailed Table of Contents
88	Table of Contents: Detailed Table of Contents
89	Table of Contents: Detailed Table of Contents
90	Table of Contents: Detailed Table of Contents
91	Table of Contents: Detailed Table of Contents
92	Table of Contents: Detailed Table of Contents
93	Table of Contents: Detailed Table of Contents
94	Table of Contents: Detailed Table of Contents
95	Table of Contents: Detailed Table of Contents
96	Table of Contents: Detailed Table of Contents
97	Table of Contents: Detailed Table of Contents
98	Table of Contents: Detailed Table of Contents
99	Table of Contents: Detailed Table of Contents
100	Table of Contents: Detailed Table of Contents

# TABLE OF SYMBOLS AND ABBREVIATIONS

$\vec{F}$	- force
$e$	- charge on electron
$\vec{v}$	- velocity
$\vec{B}$	- magnetic flux density
$r$	- radius
$\vec{p}$	- momentum
$E$	- energy in Mev
$m_0$	- rest mass of the electron
$c$	- velocity of light
$h$	- Planck's constant
$\gamma$	- frequency
$\alpha$	- fine structure constant
$N$	- Avogadro's number
$A$	- atomic weight
$Z$	- atomic number
$r_e$	- radius of the electron
$\ln$	- logarithm to the base 2.718
$\epsilon_0$	- critical energy
$\ell$	- radiation length
$t$	- thickness in radiation lengths
$n$	- number of particles
$I$	- light intensity
$\lambda$	- wave length
$\beta$	- ratio of velocity to the speed of light
$n$	- index of refraction
$T$	- tension in grams
$I$	- current in amperes
$w_{1/2}$	- width at half maximum
$\theta$	- angle
$\nu$	- dispersion value
$\text{\AA}$	- angstroms
Mev	- million electron volts
Bev	- billion electron volts
$\mu$	- electron mass





# CHAPTER I

## INTRODUCTION

The theory of the total-absorption spectrometer for gamma rays and electrons is outlined. A description is given of a lead-glass spectrometer, depending on Cherenkov radiation, which has experimentally shown an approximately linear response for energies ranging from 42 to 319 Mev with a resolution, above 200 Mev, of about 30 percent. It is believed that the useful range of this spectrometer will extend to several Bev.

Experiments in nuclear physics and high-energy physics often require that the energy of electrons and gamma rays be determined. This has been done most conveniently in the past through the use of a magnetic pair spectrometer. Electrons passing between the pole faces of a magnet are deflected in accordance with the relation

$$\vec{F} = e \vec{v} \times \vec{B} \quad (1)$$

in a circular path of radius

$$r = \frac{p}{Be} . \quad (2)$$

The energy of each electron is given by

$$E = Bcer . \quad (3)$$

Gamma-ray energies may be determined similarly by passing the rays through a converter which transforms the photons into a positron and electron pair according to

$$E_{\gamma} = h\nu = 2m_0c^2 + E_1 + E_2 . \quad (4)$$

As energies of the particles increase, larger magnets and higher currents are required, until the spectrometer becomes inconveniently large in terms of weight, cost, and power consumption. For example, a one-Bev electron requires a magnet weighing ten tons to deflect it  $30^\circ$  in a 7.3-foot radius in a field of 15,000 gauss.(4) As the energy increases, the bending radius increases proportionately, while the weight increases as the cube of the energy.

# SECTION 1 INTRODUCTION

The theory of the photoelectric effect, which is the subject of this paper, is one of the most important and interesting in physics. It is a subject which has attracted the attention of many of the greatest scientists of our time. The theory of the photoelectric effect is one of the most important and interesting in physics. It is a subject which has attracted the attention of many of the greatest scientists of our time.

The theory of the photoelectric effect is one of the most important and interesting in physics. It is a subject which has attracted the attention of many of the greatest scientists of our time. The theory of the photoelectric effect is one of the most important and interesting in physics. It is a subject which has attracted the attention of many of the greatest scientists of our time.

$$(1) \quad \nu = \frac{c}{\lambda}$$

where  $\nu$  is the frequency of the light

$$(2) \quad \nu = \frac{c}{\lambda}$$

The energy of each photon is given by

$$(3) \quad E = h\nu$$

where  $E$  is the energy of the photon,  $h$  is Planck's constant, and  $\nu$  is the frequency of the light. The energy of each photon is given by  $E = h\nu$ .

$$(4) \quad E = h\nu$$

The energy of the photon is given by  $E = h\nu$ . The energy of the photon is given by  $E = h\nu$ . The energy of the photon is given by  $E = h\nu$ . The energy of the photon is given by  $E = h\nu$ . The energy of the photon is given by  $E = h\nu$ .



At the Bevatron protons may be accelerated to 6.2 Bev in energy. These protons interact with nuclei, giving protons, neutrons, heavier nuclear fragments, pi mesons, photons, hyperons, and other short-lived particles. Magnets are required when photographic emulsions and cloud chambers are used to analyze these high-energy particles. In addition the density of the stopping medium in emulsions, cloud chambers, and even bubble chambers is low, requiring large extents of material and unwieldy experimental setups. The atomic number of the medium is low and there is small probability of observing an energetic particle until it has lost all its energy by some means of interaction.

A smaller and less costly device is therefore needed to analyze high-energy particles. A device is herein described which is believed to be capable of determining the energy of several-Bev gamma rays or electrons. This total-absorption spectrometer depends upon cascade showers to absorb the energy of the incident photon, upon the phenomenon of Cherenkov radiation to detect the energy absorbed, and upon photomultipliers to determine the amount of this radiation in the region of the visible spectrum. The gamma-ray cascade showers and their accompanying Cherenkov radiation occur in a block of lead glass 14 inches in length and 12.25 inches in diameter. The Cherenkov light emitted in this process is detected by four five-inch photomultipliers. The outputs of these photomultipliers are added and the result analyzed by a ten-channel pulse-height analyzer which operates only when a fourfold coincidence has been observed between the photomultiplier tubes. It has been found by calibration that the resulting pulses are linearly related to the energy of the incident photon or electron. For purposes of calibration gamma rays were obtained at the 335-Mev University of California Radiation Laboratory electron synchrotron, where they were converted to electron-positron pairs. Monoenergetic electrons with an energy determined by the magnetic field of a magnetic pair spectrometer entered the lead glass, giving rise to the radiation which formed a voltage pulse in the photomultiplier output circuits. The value of this pulse was proportional to the energy of the shower-initiating electron. The plot of relative pulse height versus electron energy is



linear from 42 to 319 Mev. This electron calibration can be used in gamma-ray analysis, as showers initiated by electrons and gamma rays of the same energy are almost similar in size and extent.

These items are on the list. The entire collection can be used in  
general way, as they are included by the list and the list  
of the items are listed on the list and the list.



## CHAPTER II

### THEORY

The production of cascade or multiply produced showers depends upon the interaction of charged particles and gamma rays with matter. (5) These may each interact with matter in three important ways. A charged particle or electron whose closest approach to an atom is a large distance in comparison with the size of the atom produces an excitation of the atom. When the distance of closest approach is of the order of magnitude of the size of the atom, the particles interact not with the whole atom but with the individual atomic electrons, often causing one or more to be emitted with considerable energy. With even smaller distances of approach, the interaction of the particle is with the electric field of the nucleus, and although quanta of low energy are most often emitted, occasionally a quantum of energy comparable to the energy of the particle is emitted. The more energetic the incident particle, the more likely is this bremsstrahlung radiation to be emitted. Of course a small amount of energy is also lost by electrons in the form of Cherenkov radiation. Low-energy photons interacting with an atom as a whole are completely absorbed in the production of photoelectrons. Higher-energy photons interact with electrons, producing a recoil electron and photon by the Compton effect. Still higher-energy photons interact with the Coulomb field of the nuclei, producing electron and positron pairs. The more energetic the photon or gamma ray, the more likely is the latter process.

Interacting with matter, an energetic charged particle then produces an energetic gamma ray which subsequently undergoes pair production. Each of these particles may produce bremsstrahlung gamma rays which in turn produce more pairs. In each step the number of particles increases while the average energy decreases. Eventually the energy of the electrons is reduced to the point where collision losses predominate and shower production ceases.

Important terms in the study of showers are radiation length and critical energy. On the average, a radiation length  $\ell$  may be considered as that distance in the absorber in which an electron has lost  $1/e$ th of



its energy by radiation (6). The critical energy  $\epsilon_0$  of a substance is approximately that energy at which radiation losses and collision losses of electrons are equal. The radiation length in a material is approximately proportional to  $A/Z^2$ , while the critical energy varies inversely as the atomic number  $Z$ . More exactly, the radiation length  $\ell$  in grams per square centimeter is defined as

$$\frac{1}{\ell} = 4 \alpha \frac{N}{A} Z (Z + 1) r_e^2 \ln (183 Z^{-1/3}) / \left[ 1 + .12 \left( \frac{Z}{82} \right)^2 \right]. \quad (5)$$

The critical energy may be approximately determined from the equation

$$\epsilon_0 = \frac{800}{Z}, \quad (6)$$

or, more exactly, from (7)

$$\epsilon_0 = 0.153 \ell_t \sum_{i=1}^n \frac{Z_i}{A_i} \rho_i \left( 23 + 2 \ln \frac{\epsilon_0}{\mu_e Z_i} \right). \quad (7)$$

According to the crude model by Heitler (8), an electron of energy  $E_0$  much greater than  $\epsilon_0$ , incident upon matter, will give rise to one electron and one photon after one radiation length of passage. In the second radiation length the secondary electron produces an electron-photon pair and the secondary photon an electron-positron pair, so that in  $t$  radiation lengths the total number of electrons and photons will be

$$n = 2^t \quad (8)$$

and the energy of each particle

$$E = E_0 2^{-t}. \quad (9)$$

Generally the number of photons or electrons at first increases exponentially with depth. The maximum number of particles occurs at a thickness of about  $\ln (E_0/\epsilon_0)$ . The total number of shower particles at the maximum is approximately proportional to  $E_0/\epsilon_0$ .

In order to explain the operation of this spectrometer we need a few words about Cherenkov radiation (9). The Russian, Cherenkov, discovered in 1934 that a charged particle passing through matter caused light emission. Frank and Tamm (10) explained that the effect was an electromagnetic shock wave produced as long as the particle traversed



its energy by radiation (6). The critical energy  $\epsilon_c$  is a function of the material and is approximately that energy at which the electron loses its energy by radiation in a single collision. The critical energy  $\epsilon_c$  is approximately  $610/\epsilon$  MeV, where  $\epsilon$  is the atomic number of the material. The critical energy  $\epsilon_c$  is approximately 1.02 MeV for lead.

$$(7) \quad \frac{dN}{dx} = \frac{1}{\epsilon} \left( \frac{dN}{dx} \right)_{\text{rad}} + \left( \frac{dN}{dx} \right)_{\text{ion}} + \left( \frac{dN}{dx} \right)_{\text{brems}}$$

The critical energy  $\epsilon_c$  may be approximately determined from the equation

$$(8) \quad \frac{dN}{dx} = \frac{1}{\epsilon} \left( \frac{dN}{dx} \right)_{\text{rad}} + \left( \frac{dN}{dx} \right)_{\text{ion}} + \left( \frac{dN}{dx} \right)_{\text{brems}}$$

$$(9) \quad \frac{dN}{dx} = \frac{1}{\epsilon} \left( \frac{dN}{dx} \right)_{\text{rad}} + \left( \frac{dN}{dx} \right)_{\text{ion}} + \left( \frac{dN}{dx} \right)_{\text{brems}}$$

According to the crude model of Heitler (1), an electron of energy  $\epsilon$  will produce about  $\epsilon/\epsilon_c$  secondary electrons, which will give rise to about  $\epsilon/\epsilon_c$  secondary electrons, and so on. The total number of electrons produced in a cascade of energy  $\epsilon$  is approximately  $\epsilon/\epsilon_c$ . The total number of electrons produced in a cascade of energy  $\epsilon$  is approximately  $\epsilon/\epsilon_c$ .

$$(10) \quad \frac{dN}{dx} = \frac{1}{\epsilon} \left( \frac{dN}{dx} \right)_{\text{rad}} + \left( \frac{dN}{dx} \right)_{\text{ion}} + \left( \frac{dN}{dx} \right)_{\text{brems}}$$

Generally the number of electrons in a cascade is first increased rapidly and then slowly. The maximum number of electrons in a cascade is approximately  $\epsilon/\epsilon_c$ . The total number of electrons produced in a cascade of energy  $\epsilon$  is approximately  $\epsilon/\epsilon_c$ .

In order to explain the observed results in this experiment, we used a new model (Heitler's model (1)). The critical energy  $\epsilon_c$  is approximately 1.02 MeV for lead. The critical energy  $\epsilon_c$  is approximately 1.02 MeV for lead. The critical energy  $\epsilon_c$  is approximately 1.02 MeV for lead.



the dielectric medium at a velocity greater than the velocity of light in the medium. The spectrum of Cherenkov light emitted in this process extends over all frequencies for which the velocity of electromagnetic radiation,  $c/n$ , in the medium is less than that with which the charged particle traverses the medium. The intensity and angular distribution of this radiation are given by

$$I = 4 \pi^2 e^2 Z^2 \Delta \nu \left( 1 - \frac{1}{\beta^2 n^2} \right) \quad (10)$$

or

$$I = \alpha^2 \pi Z^2 \left( \frac{1}{\lambda_1} - \frac{1}{\lambda_2} \right) \sin^2 \theta \quad (11)$$

and

$$\cos \theta = \frac{1}{\beta n}. \quad (12)$$

Cherenkov radiation (Fig. 1) (11) may be considered to be an electromagnetic analog of the situation which occurs when a bullet travels through air at a velocity greater than the speed of sound. The pattern is the same as the two-dimensional one made by the surface bow waves of a ship. Cherenkov radiation is most readily detected by means of photomultiplier tubes.

The problem, then, is to find a material which is dimensionally large enough and dense enough to contain the entire longitudinal and lateral extent of a shower and yet be transparent to light to which the phototubes are sensitive. If a shower development is contained within such a material, the total amount of Cherenkov radiation emitted will be proportional to the energy of the initiating particle and, correspondingly, the photomultiplier output pulse will be proportional to this energy (4). Essentially all the energy of the particle is contained within the shower medium; hence the name, total-absorption spectrometer.

Two large cylinders of special lead glass were acquired by the University of California Radiation Laboratory in the summer of 1954. The counter to be described is intended for use in gamma-ray spectroscopy at the Bevatron and at the converted cyclotron. The glass cylinders, cast and polished on the faces by the Corning Glass Works, have the characteristics delineated in Table I.



For estimation of the effectiveness of the glass in containing the energy of a particle, the radiation length of each element in the glass was calculated and weighted according to composition. The value of the total radiation length  $\ell_t$  was obtained by utilizing the formula

$$\frac{1}{\ell_t} = \frac{1}{\ell_{\text{P13}}} + \frac{1}{\ell_{\text{O}}} + \frac{1}{\ell_{\text{Si}}} + \frac{1}{\ell_{\text{K}}} + \frac{1}{\ell_{\text{Na}}} . \quad (13)$$

The radiation length was found to be 2.81 cm. The critical energy was determined by use of Eq. (7) to be about 18 Mev. According to Rossi (5) the behavior of all materials is approximately the same when lengths are expressed in radiation lengths and when energies are expressed in units of critical energy. Using the similarity rule of Kantz and Hofstadter (4), we see that the behavior of the glass at 430 Mev corresponds to the behavior of lead at 185 Mev. The 14-inch length and 12.25-inch diameter of this glass contain about 85% of the energy of a 430-Mev electron. At higher energies less than this percentage of the energy would be contained. Gamma-ray showers are similar to electron showers except that approximately one additional radiation length of material is required to initiate the shower. (12) Therefore a slightly smaller amount of the energy of a 430-Mev gamma ray would be contained within the glass.

Let us estimate the effectiveness of the glass in a very crude fashion. It may be seen from Fig. 2 that an electron does not emit Cherenkov radiation in this glass if it has an energy of less than 0.125 Mev. An electron in a shower is degraded in energy in accordance with Eq. (9). According to this equation the Cherenkov light will be contained in the glass cylinders for an electron whose initial energy is 780 Mev. This value compares only very roughly with the energy calculated by use of the similarity rule of Kantz and Hofstadter.

Considering an initiating electron of 3 Bev energy and utilizing Table (6) in Reference (16) we find in yet another fashion that about 85% of the electrons to be found in glass of infinite length with an energy greater than 0.5 Mev will be contained in this glass, which is 12.6 radiation lengths long. It is felt that the upper energy limit of this spectrometer can only be determined by further experimentation.





It is seen that the Cherenkov light in the glass for  $\beta = 1$  is emitted at an angle of  $52.6^\circ$ . The glass is wrapped in aluminum foil to reflect and thus retain the majority of the light that escapes from the cylindrical walls at this angle of emission.

It is seen that the characteristic light to the right of  $\lambda = 1.1 \mu$  is provided at the angle of  $25^\circ$ . The characteristic spectrum is shown and to follow and that shows the transition in the light spectrum from the cylindrical wave to the light of the light.

### CHAPTER III

#### PHOTOTUBES

The Dumont type 6364 tube is a ten-stage photomultiplier of the end-window type having an S-4 spectral response with a maximum at about 4000A, and about 75% of this response at 5000A. The glass envelope is 5.25 inches in diameter and the active photocathode surface at least 4.18 inches in diameter. The active dynode surfaces are of the silver-magnesium type, which is more stable under conditions of high current than the cesium-antimony surface used on the photocathode. The tube has an average sensitivity of 60 microamperes per lumen. The maximum allowable voltage between anode and cathode is 1800 volts. The average anode current is five milliamperes and the average anode dissipation is 0.5 watt. The average amplification at 105 volts per stage is 150,000. In this experiment, using the circuit shown in Fig. 3b, the typical signal output has been about 0.03 volt in magnitude.

This photomultiplier is extremely sensitive to magnetic fields. The counting rate varies over a wide range with the orientation of the tube in the earth's magnetic field, which is only 0.5 gauss. Operation in the pulsing field of the Bevatron at a location where the field reaches a maximum of 50 gauss presented a serious magnetic shielding problem. The proper amount of shielding to be used was determined by operating a 6364 photomultiplier with a 1/8-inch-thick plastic scintillator disc on its face in contact with a small strontium-90 electron source. A counting rate was obtained with the Bevatron magnet turned off. The value of the Bevatron magnetic field surrounding the shielding of the phototube was varied during the field cycle with a multivibrator gating circuit. After many different trials with different geometric arrangements a suitable magnetic shielding configuration was found. The Bevatron field varies from zero to a maximum during a time of about 1.5 seconds at a rate of about ten cycles per minute. The counter was set to operate for 0.1 second during various stages of the pulse. The same counting rate was maintained at the location where the spectrometer was to be used for all values of the magnetic field. With a 5/8-inch-





thick 12-inch-diameter annealed soft iron cylinder outside 0.025-inch-thick  $\mu$ -metal that surrounded the phototube, the field inside the  $\mu$ -metal was reduced to less than 0.02 gauss, although the field outside the iron, as measured with an R. F. permalloy strip magnetometer was 50 gauss. The photomultiplier operated satisfactorily under these conditions. The  $\mu$ -metal was effective only if the field was first reduced to less than ten gauss by the soft iron. It was also found to be important to have the  $\mu$ -metal extend several inches forward from the plane of the photocathode.

After several trials the circuit shown in Fig. 3a was selected for use with the available electronic equipment. Best operation (maximum counting rate) was obtained when the photocathode was connected directly to the internal shield so that the two were at the same potential. To reduce input capacitance noise, the photocathode was carried at a negative high potential of about 1200 volts. To obtain optimum collection of the electrons at the first dynode, the resistor between the photocathode and the first dynode was made larger than the resistors between the remaining dynodes. The last three stages were bypassed with capacitors to maintain the last dynodes at constant potentials. The capacitors supplied the required current during the millimicrosecond pulse time, leaving the dynodes at steady potentials. The 24,000-ohm load resistor lengthened the pulse to about 0.2 microsecond across the top. The cathode follower circuit furnished an impedance match between the high-output impedance of the phototube circuit and the cable impedance of 125 ohms. This prevented ringing in the pulse. A stretched pulse was necessary to provide the proper input for the Ten-Channel UCRL pulse-height analyzer. (13)

After 12 hours, the water was removed and the plants were left to dry in the sun. The plants were then ground to a fine powder and the powder was placed in a glass bottle. The bottle was then sealed and the powder was used for the experiment. The results of the experiment were as follows: The plants which were left in the sun for 12 hours were found to be much more resistant to the action of the water than the plants which were left in the sun for 24 hours. This was due to the fact that the plants which were left in the sun for 12 hours had a much higher percentage of water in their leaves than the plants which were left in the sun for 24 hours. The plants which were left in the sun for 12 hours also had a much higher percentage of chlorophyll in their leaves than the plants which were left in the sun for 24 hours. This was due to the fact that the plants which were left in the sun for 12 hours had a much higher percentage of chlorophyll in their leaves than the plants which were left in the sun for 24 hours.

The results of the experiment were as follows: The plants which were left in the sun for 12 hours were found to be much more resistant to the action of the water than the plants which were left in the sun for 24 hours. This was due to the fact that the plants which were left in the sun for 12 hours had a much higher percentage of water in their leaves than the plants which were left in the sun for 24 hours. The plants which were left in the sun for 12 hours also had a much higher percentage of chlorophyll in their leaves than the plants which were left in the sun for 24 hours. This was due to the fact that the plants which were left in the sun for 12 hours had a much higher percentage of chlorophyll in their leaves than the plants which were left in the sun for 24 hours. The results of the experiment were as follows: The plants which were left in the sun for 12 hours were found to be much more resistant to the action of the water than the plants which were left in the sun for 24 hours. This was due to the fact that the plants which were left in the sun for 12 hours had a much higher percentage of water in their leaves than the plants which were left in the sun for 24 hours. The plants which were left in the sun for 12 hours also had a much higher percentage of chlorophyll in their leaves than the plants which were left in the sun for 24 hours. This was due to the fact that the plants which were left in the sun for 12 hours had a much higher percentage of chlorophyll in their leaves than the plants which were left in the sun for 24 hours.

## CHAPTER IV

### EXPERIMENTAL EQUIPMENT

The photograph in Fig. 4 shows the disassembled spectrometer designed by the author. The soft iron magnetic shield case, weighing about 400 pounds, rests on an aluminum dolly. The internal grooves cut in the case allow for the inclusion of from one to four cylinders of glass. The glass itself is wrapped circumferentially in aluminum foil, sheet rubber, and mu-metal before installation in the case. The glass unit then fits snugly in the case. Against one face of the glass is placed the phototube and shield-retaining disc assembly. One snap ring holds this assembly against this glass. Against the other face of the glass is placed a sheet of aluminum foil for reflection, a disc of rubber for shock protection, and one radiation length of iron in the form of a disc for magnetic shielding and gamma-ray conversion. After insertion of the set-screw retaining ring, the second snap ring is fitted into its groove. The entire assembly is held rigidly in place by tightening the set screws, which force the disc against the rubber and glass till it is firmly held against the phototube disc, which is fast against the other snap ring. Thus the spectrometer can be used in either the vertical or the horizontal position. On the end of each phototube is placed its circuit box, which has two rings (one on either side). Each phototube is pressed against the glass by two springs fastened between the circuit box and eye bolts mounted in the phototube retaining disc. Each end of the magnetic shield case has a gasket groove for a rubber gasket. This permits a lighttight seal between the case and the end covers, which are held in place with bolts. The entire assembly weighs about 800 pounds.

Each circuit box contains a high-voltage input, two signal outputs, and a filament and plate voltage supply input. These are attached by cables to cable lead-throughs in the end cover on the end away from the glass. Cables lead from the outer side of the end cover to power supplies.

To permit convenient assembly and disassembly of the device the glass is placed on a wooden disc about four inches thick on the front end and cover. Before the magnetic shield case is lowered over the





phototube-glass assembly the rear snap ring is placed in its proper groove. The case is hoisted by a crane whose sling is fastened to eye bolts in the case end. The case is lowered carefully into place over the glass assembly, the front end cover is bolted on, and the spectrometer is lowered to the horizontal position. The end cover and wooden disc are removed, the plates, set-screw ring, and front snap ring are installed.

It was found that an excellent optical bond between the phototubes and glass could be made by spreading Dow Corning 200 silicone compound between them. This material is clear and colorless, and has a viscosity of 2,500,000 centistokes, an index of refraction of 1.4, and a light transmission of more than 95% in the visible region. When the parts were tightened all discontinuities in this material disappeared and a clear optical path existed through the glass and the phototubes.

To make use of the spectrometer to measure the energy of gamma rays, one must calibrate it in some fashion to determine the relation of pulse height to incident energy. The synchrotron accelerates electrons to about 335 Mev by adding energy to them from a radiofrequency electric field. The electrons travel in a circle of almost constant radius under the influence of a magnetic field. When the radiofrequency field is turned off while the magnetic field still increases, the electrons spiral in toward the center because of the loss of energy by radiation and also because of the increasing magnetic field. These electrons strike a platinum target. The bremsstrahlung emitted passes through a collimator. The energy of these gamma rays ranges from zero to the maximum energy of the electrons striking the target. These gamma rays strike a converter, giving electrons which pass through a large pair spectrometer magnet as shown in Fig. 5.

The pair spectrometer magnet can deflect 330-Mev electrons about  $35^\circ$  when it is operated at a field strength of 12,000 gauss. The electron energy associated with a particular orbit and current of the magnet can be determined by using a fine wire which carries a known current and is under a known tension. Such a wire will follow the orbit given by the equation





$$E = 2.97 \text{ T/I} . \quad (14)$$

With a fixed entrance slit formed by the magnet yoke, the point of exit is determined for electrons of a particular energy at a certain field value. It is possible by changing the magnet current to make electrons of various energies emerge from this collimated exit slit according to the simple relation

$$B \propto I \propto E. \quad (15)$$

The relation holds for relativistic particles. The range of energies of electrons emerging from the pair spectrometer at any given setting of the magnet current can be narrowed by narrowing the exit slit. The uncertainty in the energy of the electrons emerging from the exit slit is about  $\pm 5$  percent. These errors are due to friction in the wire orbit weight pulley, lack of parallelism of the orbit wire with the incident gamma rays, inaccuracies in the current measurement, the finite width of the entrance and exit slits, and inaccuracies in the magnet current setting.

These monoenergetic electrons were permitted to enter the Cherenkov counter axially. The peak in pulse-height output obtained through the use of the electronics shown in Fig. 6 was supposed to shift its value linearly with the incident electron energy. The output pulse of each photomultiplier was lengthened and then fed into a cathode follower circuit to match the 150-foot cable impedance. One output from each cathode follower was fed to a linear amplifier while the other output led into a four-channel adder. The output of each linear amplifier went through a variable gate and delay unit, which activated the quadruple coincidence mixer. The mixer output was passed through another gate and delay, which furnished a signal for the triple-coincidence unit of the UCRL ten-channel pulse-height analyzer. The adder output went through another linear amplifier and into the triple coincidence of the pulse-height analyzer through its associated circuitry. The third input to the triple coincidence came from the synchrotron scaler gate and beam monitor, which allowed the analyzer to count only during the 3-millisecond interval during which the electron beam appeared six times





per second. This gate is necessary to eliminate injector and magnet noise, which are very prevalent at the synchrotron.

The UCRL ten-channel analyzer functioned briefly as follows. The window amplifier section permitted the bottom of its signal output to be subtracted away or the entire signal to be expanded, providing a means of varying the channel widths. A sliding pulse generator, when operated at a constant pulse height through a precision decade resistor, permitted the initial establishment of window widths of any amplitude. Since this fed into the linear amplifier after the adder, nonlinearities in the adder amplifier were eliminated by adjusting individual discriminators to accept the calibrated pulses from the pulse generator. The sliding pulse generator has the additional very important function of checking the exact widths of the channels in the pulse-height analyzer. Occasionally during the taking of data, the sliding pulser is fed into the analyzer through the adder linear amplifier and caused to slide by means of a precision motor-driven resistor in such a way that if the channels are set to equal widths, they will record equal numbers of counts from the sliding pulser. If they do not, the appropriate correction factors are determined from this pulsing. Since it is not desired to count the signal pulse before its maximum height is reached, the timing-pulse generator delays its output till after the window amplifier signal pulse has been at its maximum for 2.5 microseconds. This pulse is stretched to insure that it keeps its correct height till after the coincidences take place. The signal pulse fires all discriminators through the channel corresponding to the height of the pulse. Each discriminator gives a positive coincidence pulse and a negative anticoincidence pulse. The timing pulse gets to the anticoincidence circuit of each scaler, but will not pass through the anticoincidence unless the discriminator of that scaler has not fired. This anticoincidence output feeds to the coincidence circuit of the next lower unit. If the discriminator of this unit has fired, the coincidence pulse is counted in that channel only.





## CHAPTER V

### EXPERIMENT AND RESULTS

Before the magnetic shield case and other parts were completed one cylinder of glass was mated with one phototube and the output pulses were analyzed in the pulse-height analyzer. The signals were supposedly coming from cosmic rays. The noise of one tube was measured by taking a pulse-height curve with the phototube covered with lighttight paper. The phototube dark current and thermal noise so masked the desired effect that the only conclusion that could be drawn was that the tube noise occurred at the same rate as the cosmic ray counts in the lower pulse-height channels. The signal-to-noise ratio improved, however, as the subtractor level of the pulse-height analyzer was raised. It was found that, other conditions remaining the same, the counting rate increased by a factor of four when the DC 200 compound was used for an optical bond. The signal-to-noise ratio obtained with the phototube on top of the glass looking down and receiving vertically reflected light from the aluminum reflector under the glass was only one-fourth as great as with light from cosmic ray showers directly incident upon the tube through the glass when the tube was under the glass looking up. This result indicated that the aluminum reflector was effective.

At this point it should be remembered that cosmic rays fall upon the earth at all angles but in largest numbers from the vertical direction at an average rate of one per square centimeter per minute. Assuming that the glass cylinders present a plane surface to these rays we see that, since the area is 12.25 by 14 inches, a maximum cosmic ray counting rate of 18.4 per second could be obtained. Fig. 7 shows that the observed counting rate, obtained with the output of four tubes operated in coincidence, of 9.4 per second is well within this limit. The shape of Fig. 7 is explained as follows. The electrons and gamma rays produce showers of varying sizes in the glass according to their energy. These showers give pulse heights of all sizes. Mu mesons, however, as they have an average energy of one Bev at sea level, possess a small muon-nucleon cross section, and have minimum ionization loss (14), do not in

EXPERIMENTAL RESULTS

The first experiment was conducted with a view to determining the effect of the position of the glass on the rate of evaporation. The results of this experiment are given in Table I. It will be seen from this table that the rate of evaporation is not affected by the position of the glass. The second experiment was conducted with a view to determining the effect of the area of the glass on the rate of evaporation. The results of this experiment are given in Table II. It will be seen from this table that the rate of evaporation is directly proportional to the area of the glass. The third experiment was conducted with a view to determining the effect of the thickness of the glass on the rate of evaporation. The results of this experiment are given in Table III. It will be seen from this table that the rate of evaporation is not affected by the thickness of the glass. The fourth experiment was conducted with a view to determining the effect of the temperature of the glass on the rate of evaporation. The results of this experiment are given in Table IV. It will be seen from this table that the rate of evaporation is directly proportional to the temperature of the glass. The fifth experiment was conducted with a view to determining the effect of the humidity of the air on the rate of evaporation. The results of this experiment are given in Table V. It will be seen from this table that the rate of evaporation is not affected by the humidity of the air. The sixth experiment was conducted with a view to determining the effect of the wind velocity on the rate of evaporation. The results of this experiment are given in Table VI. It will be seen from this table that the rate of evaporation is not affected by the wind velocity. The seventh experiment was conducted with a view to determining the effect of the direction of the wind on the rate of evaporation. The results of this experiment are given in Table VII. It will be seen from this table that the rate of evaporation is not affected by the direction of the wind. The eighth experiment was conducted with a view to determining the effect of the time of day on the rate of evaporation. The results of this experiment are given in Table VIII. It will be seen from this table that the rate of evaporation is not affected by the time of day. The ninth experiment was conducted with a view to determining the effect of the season on the rate of evaporation. The results of this experiment are given in Table IX. It will be seen from this table that the rate of evaporation is not affected by the season. The tenth experiment was conducted with a view to determining the effect of the weather on the rate of evaporation. The results of this experiment are given in Table X. It will be seen from this table that the rate of evaporation is not affected by the weather.

the main produce showers in passing through a medium. Mu mesons all have about the same track length through the glass of about 31 cm and therefore produce Cherenkov light pulses of the same intensity. These pulses give the peak in Fig. 7. According to Winckler and Anderson (15), who observed only mu mesons, the high-energy tail of this curve is due to knock-on electrons produced by the mu mesons. In Fig. 7, however, the high-energy tail may be attributed largely to very energetic electrons and gamma rays of different energies that have produced showers in the glass. The high-energy tail was very evident in data taken by attenuating the signal input to the linear amplifier that fed the pulse-height analyzer. This procedure shifts the energy appearing in a particular channel of the pulse-height analyzer upward and increases the width of each channel by the factor of attenuation. Pulses were counted when the input to the linear had been attenuated by 20 decibels from the input existing when the cosmic ray peak was observed.

The calibration experiment was first conducted with the 0.705-inch-thick iron disc in front of the glass but with only one cylinder of glass installed. The mu-metal shields of all phototubes were electrically connected through the retaining disc so that the negative high potential of 1200 volts was the same on the photocathodes of all tubes since the shields were electrically connected to the photocathodes as well. The entire region around the photocathode must be operated at the photocathode potential to insure proper focusing of the electrons between the photocathode and first dyhode and to eliminate currents in the glass envelope. The accidental coincidence rate and the noise from all four tubes operated in coincidence had been previously found to be negligible at this potential. A 1/4-inch-thick lead converter was used in the pair magnet, whose exit was 1.25 inches in width. A 100-ampere magnet current supplied a field of about 12,000 gauss, which deflected 319-Mev electrons about  $30^{\circ}$  into the spectrometer. The background from the synchrotron was measured by blocking the exit of the pair magnet with lead. The background counting rate was negligible under the conditions of operation described above. Although an approximately linear relationship existed between the voltage of the pulse-height peak and the electron





energy, very poor resolution was obtained, and no observations were possible where the electron energy was less than 85 Mev.

To improve the resolution and to increase the pulse-height size the following changes were made. A 14-inch-diameter aluminum disc, with an eight-inch hole cut in the center, was substituted for the iron disc. The shower formation now took place almost entirely in the glass instead of partly in the iron as before. In addition, the second cylinder of glass was installed. Finally, the phototube circuit was modified as shown in Fig. 3b. This revision allowed the photocathode of each tube to be operated at ground potential. The gain of each phototube could then be adjusted to the same value by operating the tubes in double coincidence in all possible pair combinations and adjusting their high voltages until the peak in the pulse-height analyzer appeared in the same channel for each of the six pairs. The gains of the four linear amplifiers that drive the four variable gates were adjusted to be the same by equalizing their counting rates. Each pair of tubes now gave the same counting rate as well as the same peak position.

The above operation was repeated for all four combinations of three tubes in coincidence, and finally for all four tubes in coincidence. The settings of the high voltages were as follows: tube No. 1, 1150 volts; tube No. 2, 1125 volts; tube No. 3, 1260 volts; and tube No. 4, 1500 volts. It was noted that the adder output was approximately linear. The results of the calibration are shown in Figs. 8 through 14. The background counting rates, determined by placing a lead brick in the exit slit, have been subtracted. At the lowest energy point of 42 Mev the background counting rate was more than one-half the signal rate at the peak pulse-height value. The signal-to-background ratio improved with increasing electron energy until it attained a value of 32 to one at 251 Mev at the peak pulse-height value. Above this energy, background was found to be negligible.

In conducting the calibration it was not necessary to obtain data for each part of the experiment for the same integrated beam output (as measured by an ionization chamber connected to a recording electrometer) except where background and signal counts for the same energy were





being compared. In the measurement of the linearity of pulse output with energy or the change of resolution with energy, the data for different energies can be taken for different integrated beam outputs. The cosmic ray portion of the background counting rate was found to be negligible because the signal counting rate during the 6-millisecond synchrotron gate was so much larger. The total quadruple counting rate of about 1600 per second for 167-Mev electrons as calculated from the area of Fig. 11 was sufficiently small so that the accidental quadruple coincidence rate was negligible in view of the resolving time of about ten microseconds. There is a three percent chance that any particular pulse is due to showers from two electrons occurring in the glass at the same time (pileup). A plot of percent width at the half maximum shown in Fig. 15 discloses that above the 200-Mev energy value the percentage remains constant at a value of about 45 percent. If it is assumed that energies that differ by 60 percent of this value can be resolved, the resolution of the spectrometer is seen to be about 30 percent above 200 Mev. These measured resolutions, of course, are the fold of the energy resolution of the magnetic channel in the pair magnet and the natural resolution of the total-absorption spectrometer, which is made up of statistical fluctuation in the number of shower particles.

The histogram for the cosmic ray peak, Fig. 7, is especially valuable because the peak anchors a point on the calibration curve, Fig. 16. This peak, occurring at the same value as that at which 182-Mev electrons have their peak, is due to mu mesons as explained on p. 16. According to Sternheimer (7), the average track length of a photon in lead glass at 180 Mev initially is about 2.6 cm. The track length for an electron under these conditions would be about the same. The sum of the electron track lengths obtained by multiplying by the average number of electrons in the shower, as estimated from the curves in Janossy (16) is approximately 31 cm, the same as the mu-meson track length. This explains the location of the cosmic ray peak.

The fact that a finite pulse height for electrons of zero energy is indicated in Fig. 16 for a straight-line extrapolation is believed to be because the linear relationship does not hold at the low energy values.



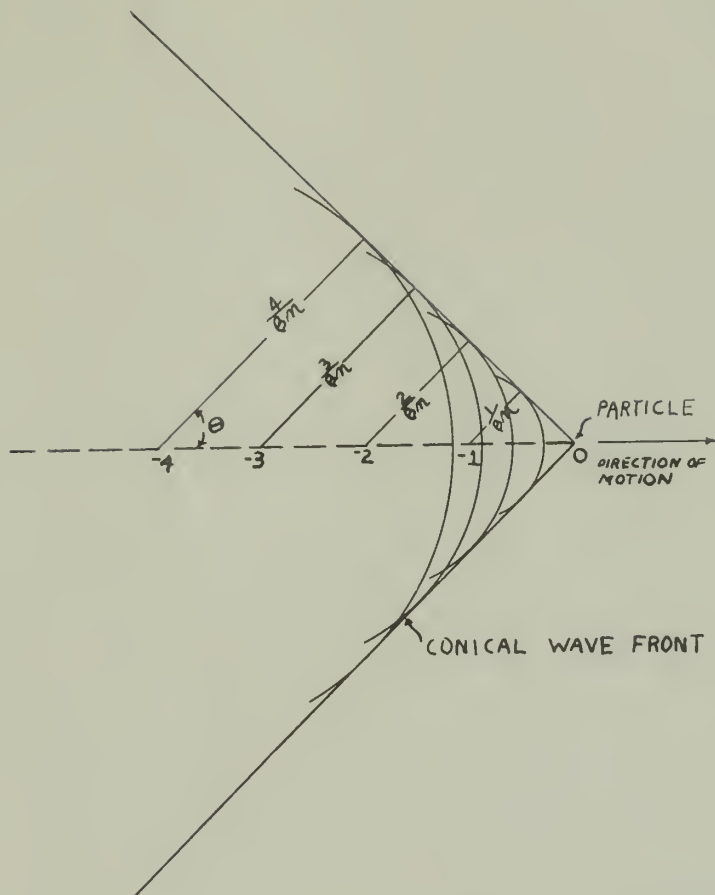
Further investigation of this region is necessary, however, before the correct relationship can be determined.

The major difficulty encountered in reproducing results has been caused by drifts in amplifier gains and in discriminator values. These drifts accounted for some of the uncertainty in the pulse height shown in Fig. 16. Major improvements can probably be made by substituting a faster coincidence circuit, by shortening the time length of the signal, by using a smaller load resistor with the anode of the photomultiplier, by adding a fast pulse stretcher after the adder, by operating under stable temperature conditions, and by pulsing through the entire circuit with a pulse of known size to determine the exact gain of each part of the experimental setup.

The calibration of this spectrometer can be carried beyond the 319-Mev point by utilizing a magnet at the Bevatron to select electrons converted from the gamma rays resulting from high-energy  $\pi^0$ -meson decays. These mesons may be produced by bombarding nuclei with high-energy protons. For example, an electron of 2 Bev energy may be deflected  $13^\circ$  in a radius of 4 meters in a 15,000-gauss field produced by the 38-ton spiral-orbit spectrometer magnet.







MU-9501

Fig. 1. Cherenkov Radiation. Huygens construction of wave front. Charged particle moving in positive  $x$  direction at velocity  $v = \beta c$ . Time required for particle to move from  $-4$  cm to  $0$ ;  $\tau = 4/\beta c$ . In time  $\tau = 4/\beta c$  light travels  $r = (c/n) \tau = 4/\beta n$  cm. Therefore wavelet starting when particle was at  $-4$  cm has radius  $4/\beta n$  when particle reaches  $0$ . Wavelets reinforce along conical wave front propagated in direction  $\theta$  relative to moving particle.  $\cos \theta = (4/\beta n)/4 = 1/\beta n$ .



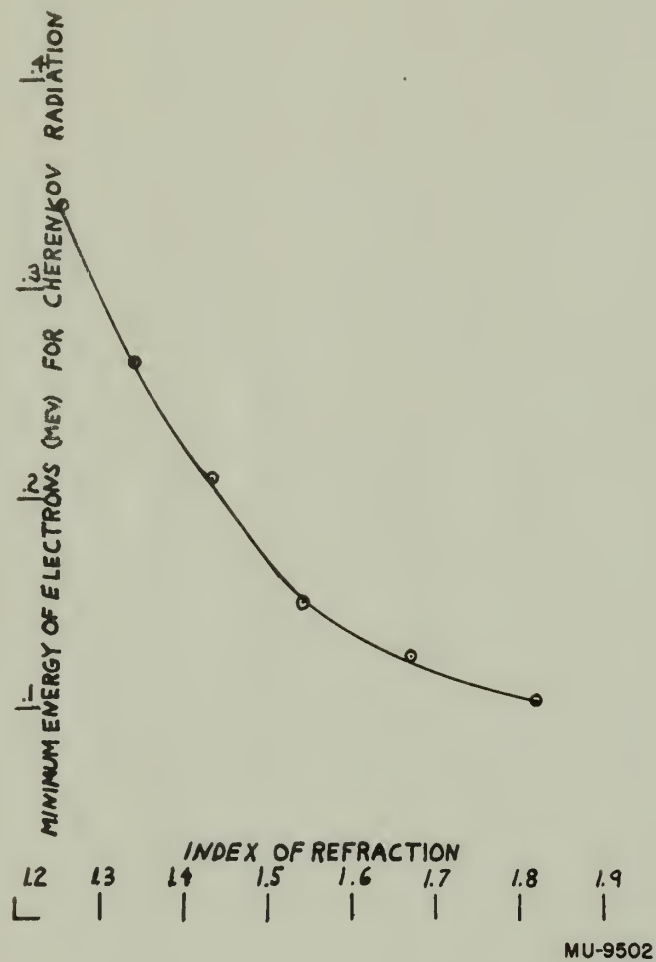


Fig. 2. Graph of the minimum energy of electrons for Cherenkov radiation versus index of refraction.

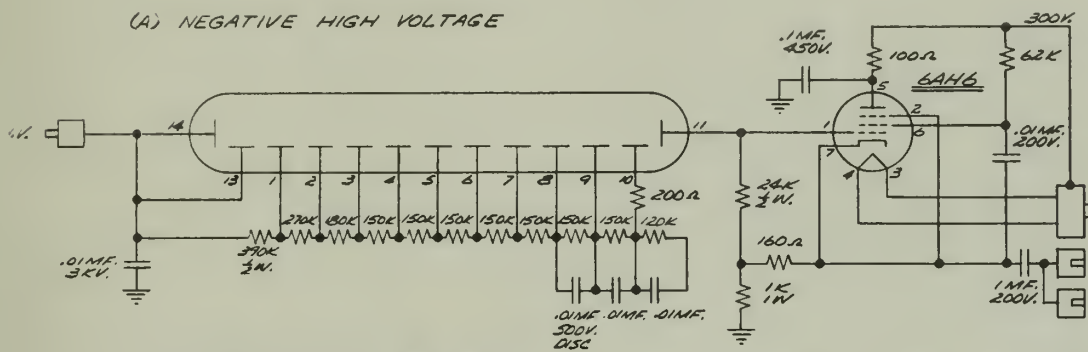


Fig. 1. Graph of the relationship between the weight of the substance and its volume.

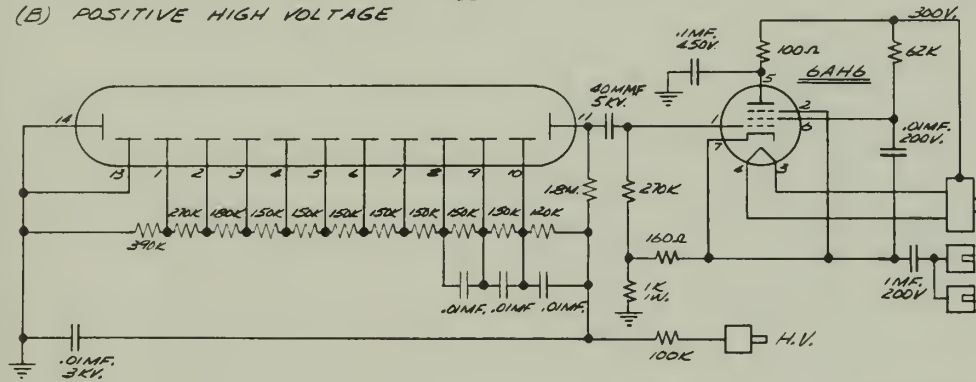


## PHOTOMULTIPLIER CIRCUITS

(A) NEGATIVE HIGH VOLTAGE



(B) POSITIVE HIGH VOLTAGE



MU-9503

Fig. 3. Photomultiplier circuits.

# FIGURE 1. Schematic diagram of the experimental setup.

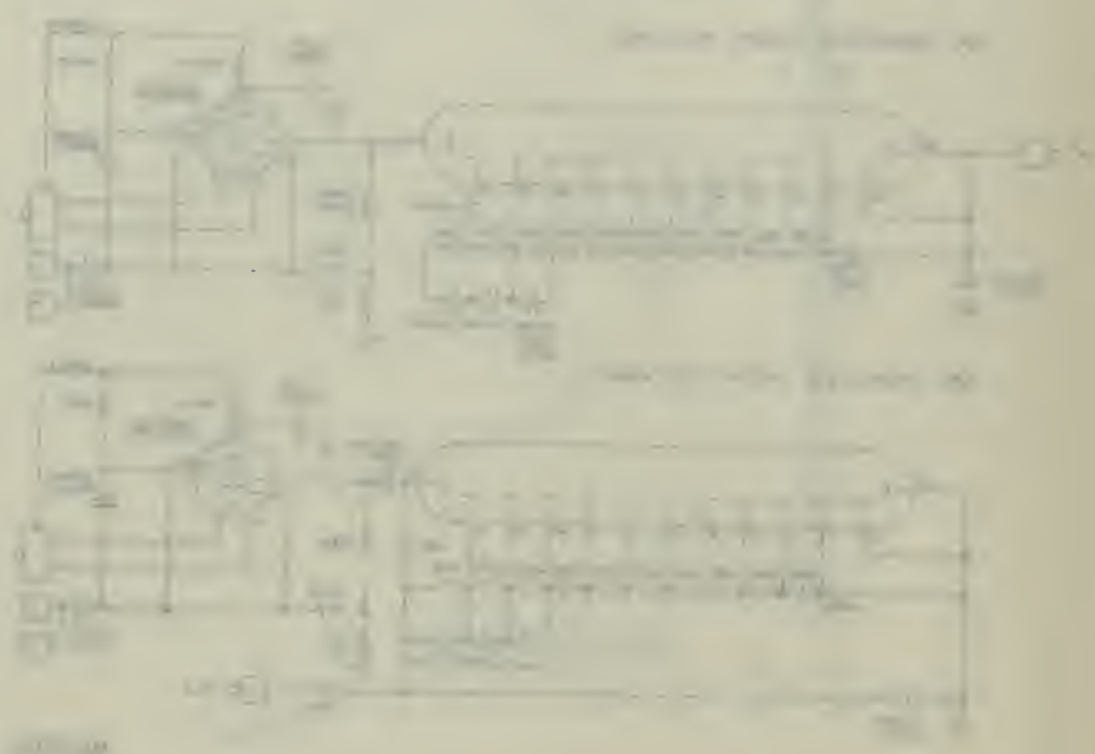


FIGURE 1. Schematic diagram of the experimental setup.

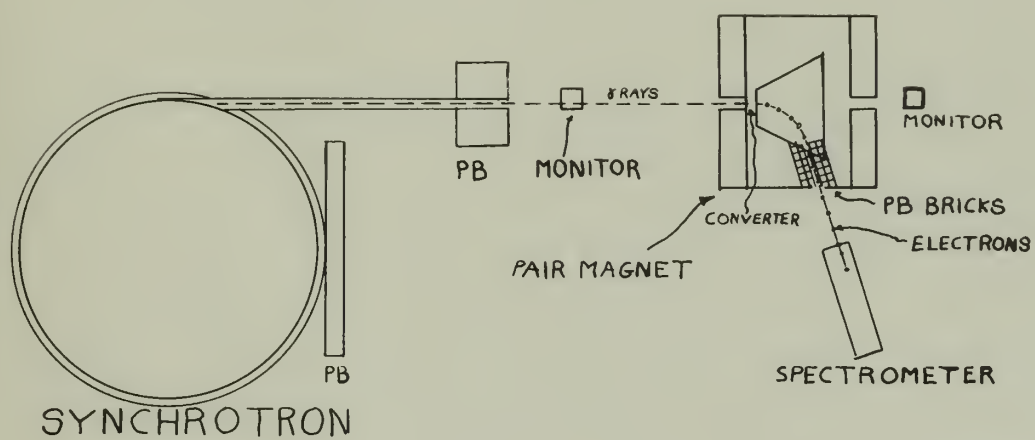


ZN-1262

Fig. 4. Component parts of the total-absorption gamma-ray spectrometer.

1988





MU-9504

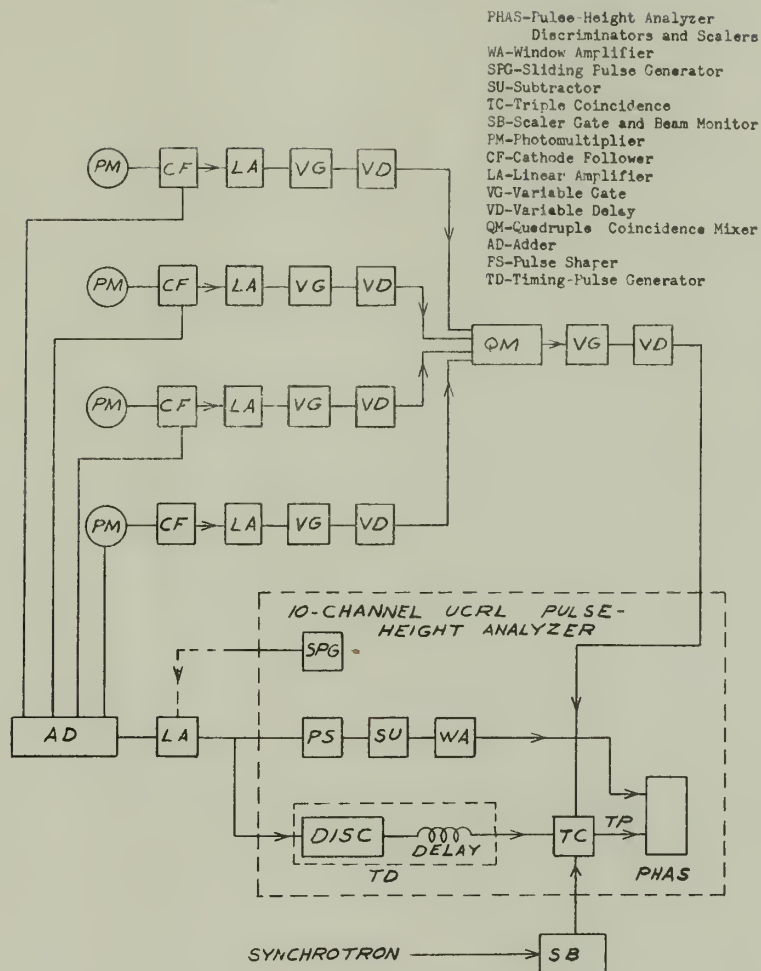
Fig. 5. Calibration layout for the spectrometer at the UCRL synchrotron.



Fig. 1. Schematic diagram of the pump and motor assembly.



# ELECTRONIC ARRANGEMENT



MU-9505

Fig. 6. Electronic arrangement.



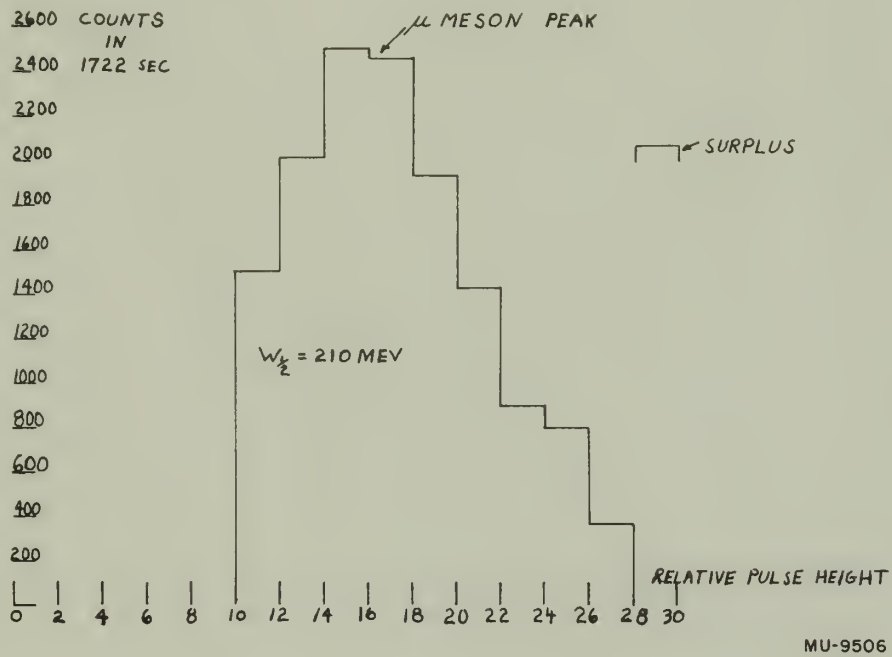


Fig. 7. Histogram of cosmic rays observed at the rate of 9.4 counts per second.



Fig. 1. Titration curve of a weak acid with a strong base. The curve shows the pH of the solution as a function of the volume of base added.

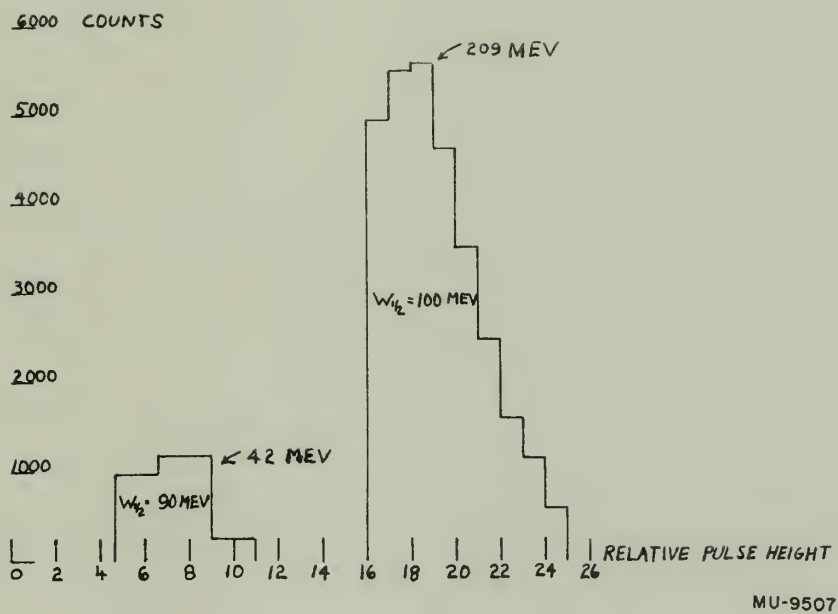
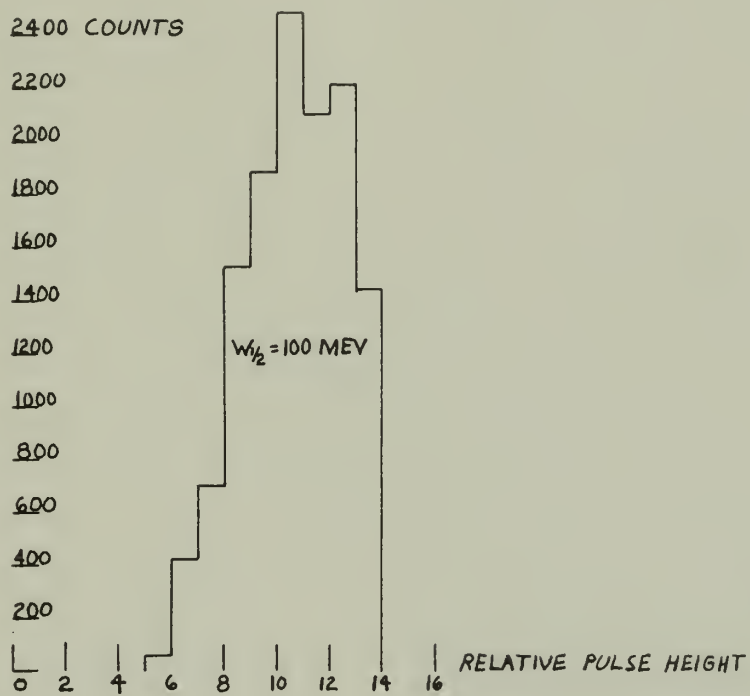


Fig. 8. Histogram of the relative pulse-height distribution of 42-Mev and 209-Mev electrons.







MU-9508

Fig. 9. Histogram of the relative pulse-height distribution of 94-Mev electrons.



FIG. 1. Distribution of counts per hour for a single channel.

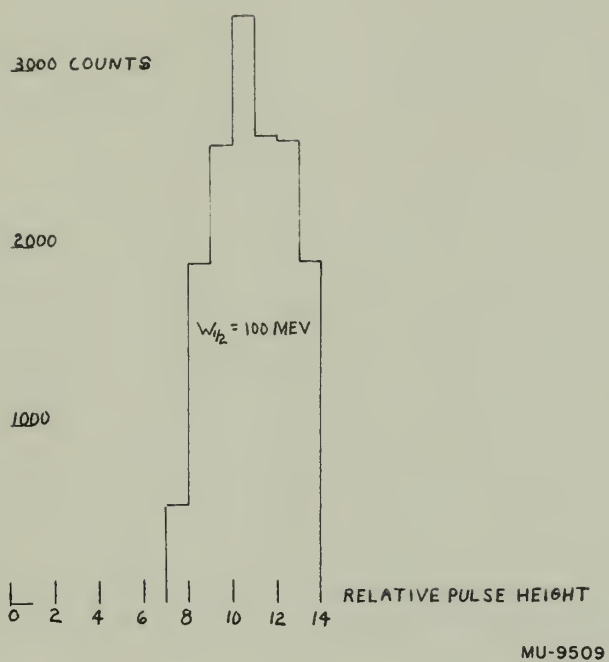


Fig. 10. Histogram of the relative pulse-height distribution of 119-Mev electrons.



Fig. 1. Relationship of refractive index and concentration of a solution of a certain substance.



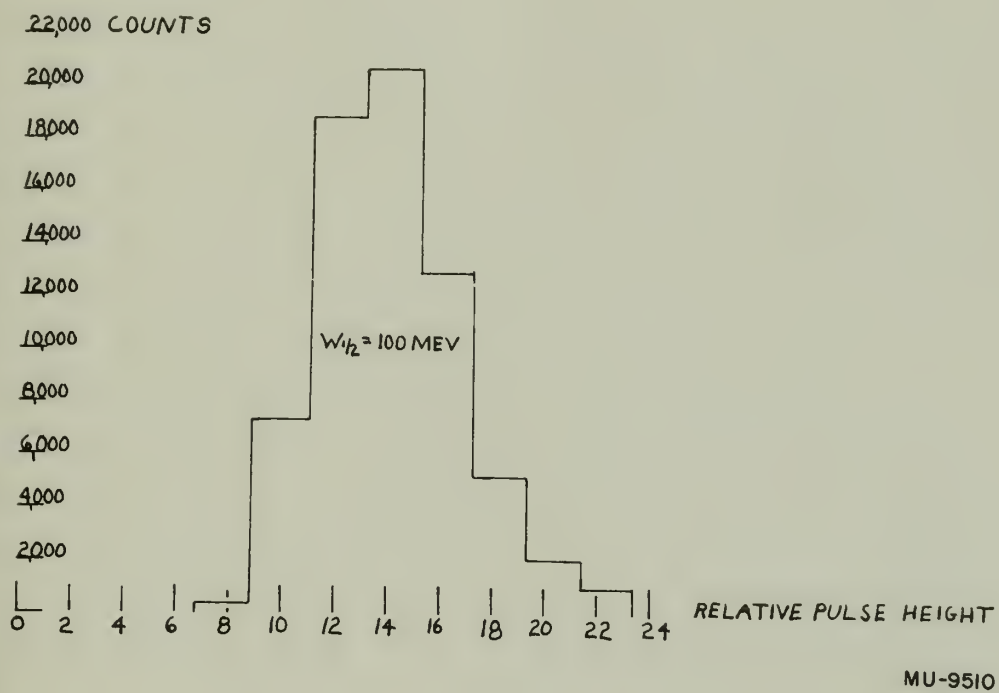
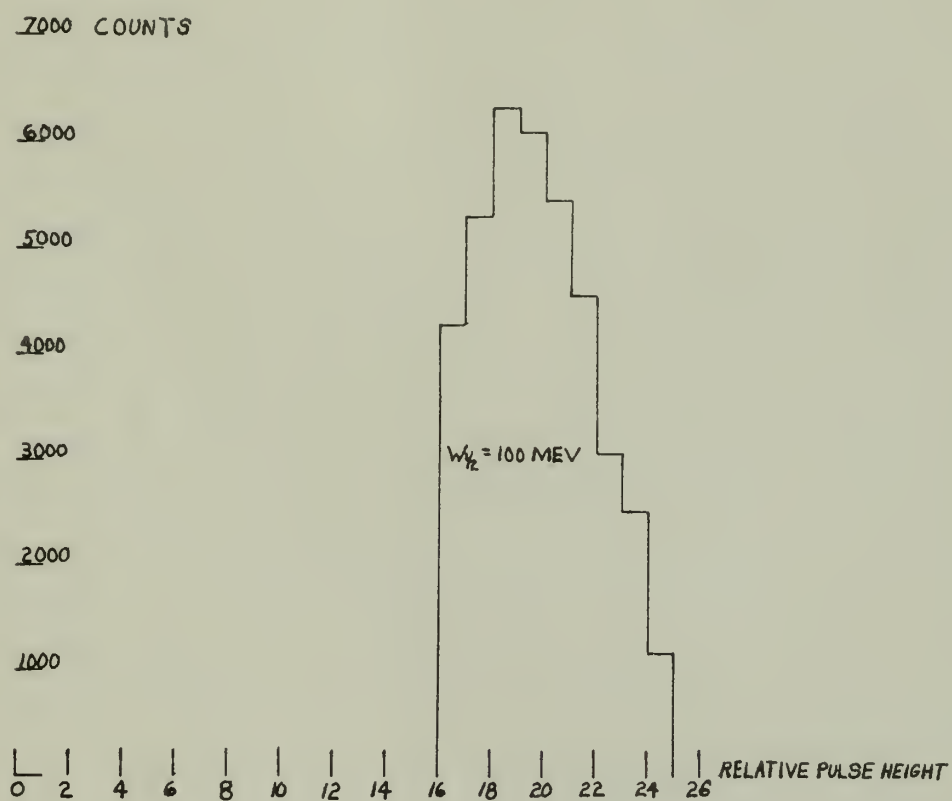


Fig. 11. Histogram of the relative pulse-height distribution of 167-Mev electrons.



Fig. 1. Relationship of the flow rate of the water and the time of the flow.



MU-9511

Fig. 12. Histogram of the relative pulse-height distribution of 228-Mev electrons.

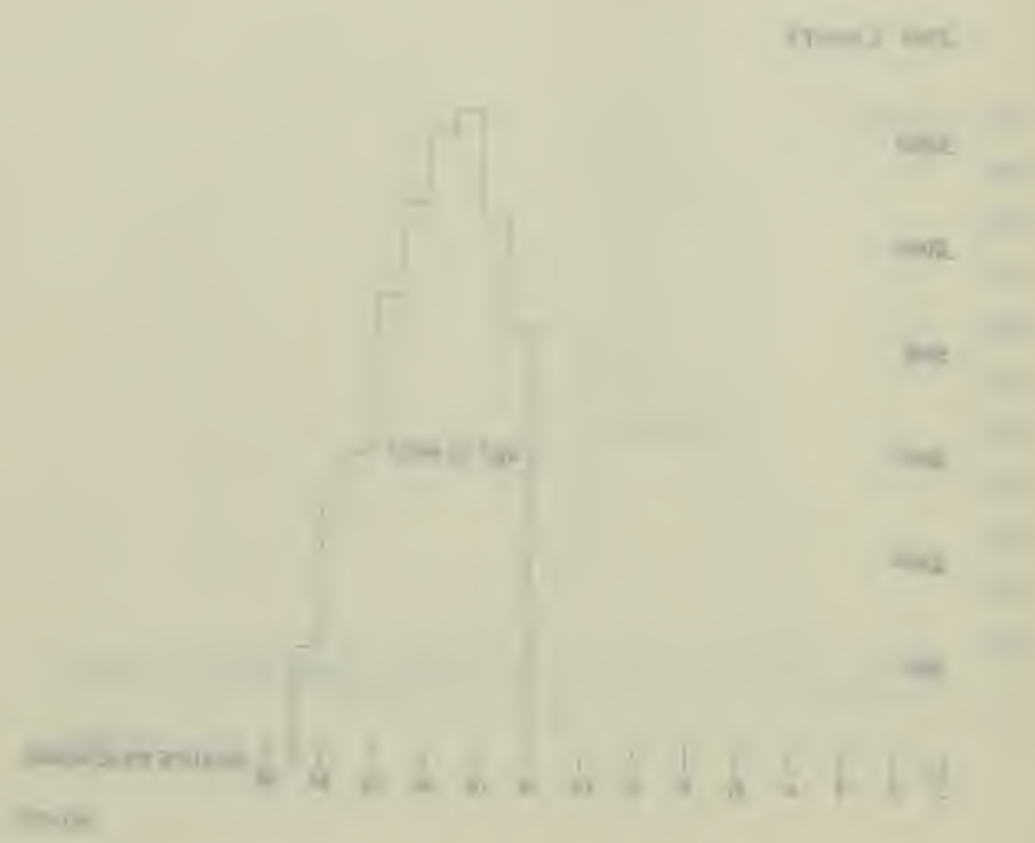


Figure 1. Frequency distribution of the number of days per week that the respondent reports being physically active.

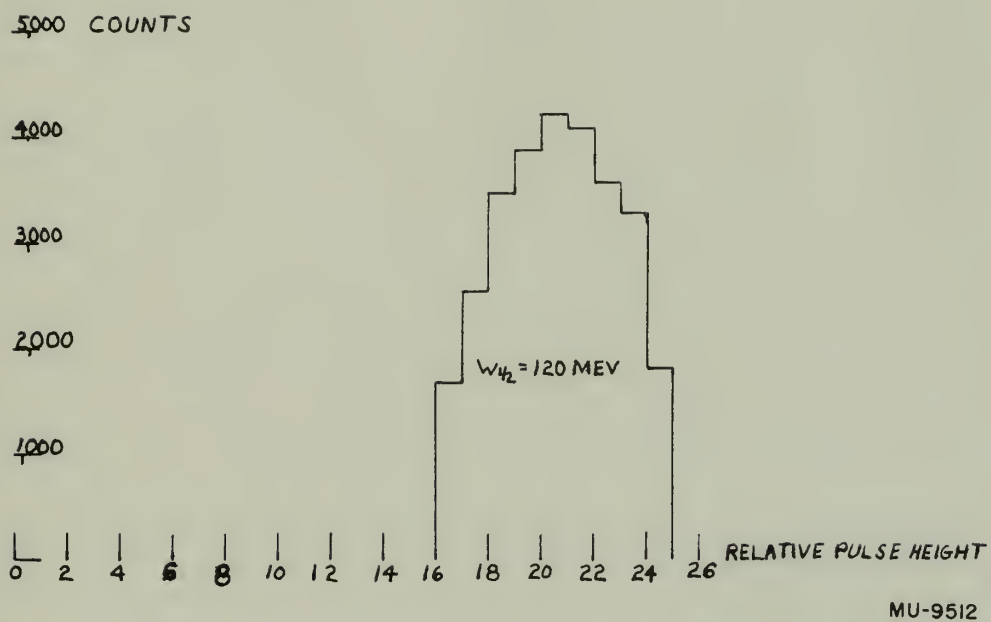


Fig. 13. Histogram of the relative pulse-height distribution of 251-Mev electrons.





Fig. 12. Histogram of the random noise signal distribution at 100 Hz.



Fig. 14. Histogram of the relative pulse-height distribution of 319-Mev electrons.

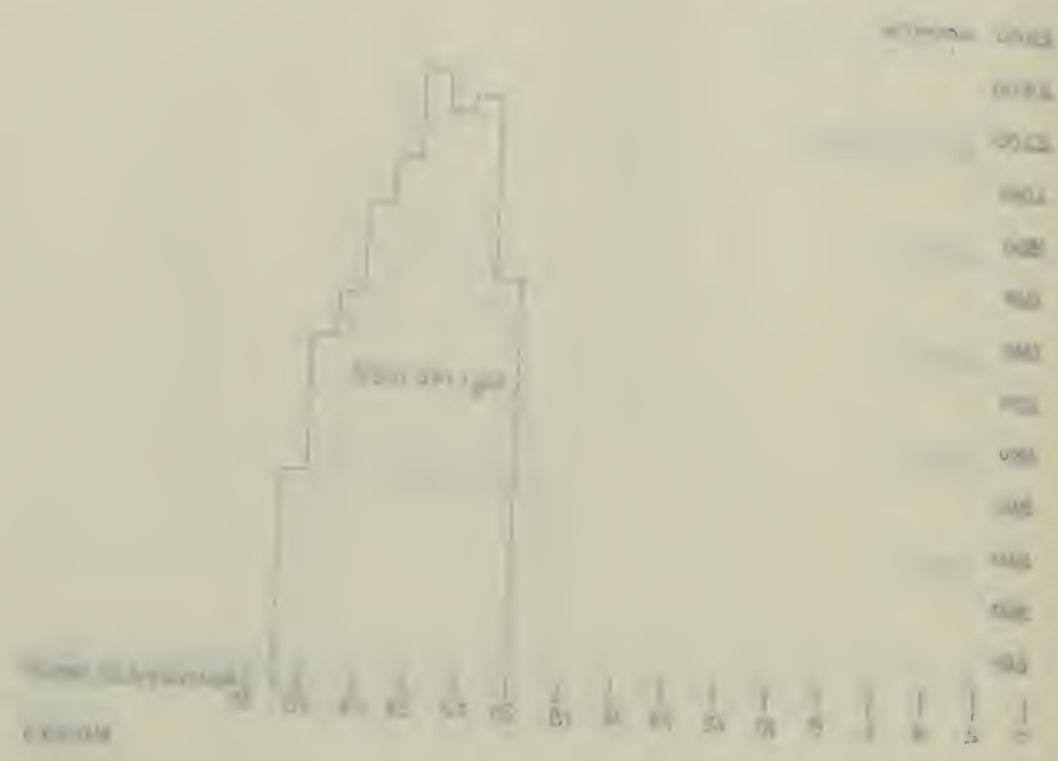


Fig. 1. Relative intensity of the relative output spectrum of the 212-MHz electron.

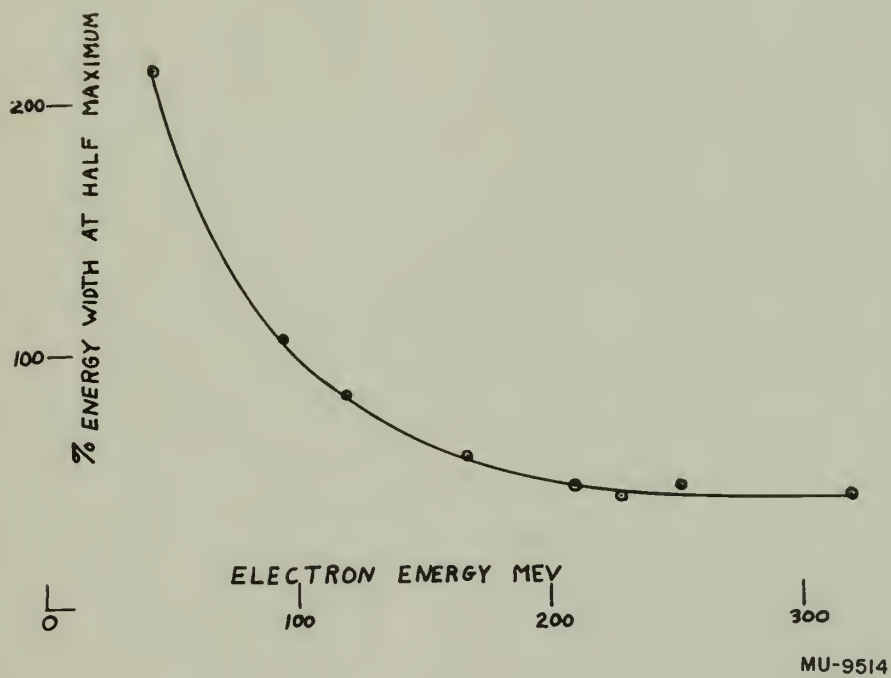


Fig. 15. Graph from which the resolution of the spectrometer may be determined.



Fig. 1. Arrhenius plot of the rate of reaction of the decomposition of hydrogen peroxide. The straight line indicates that the reaction is of first order.



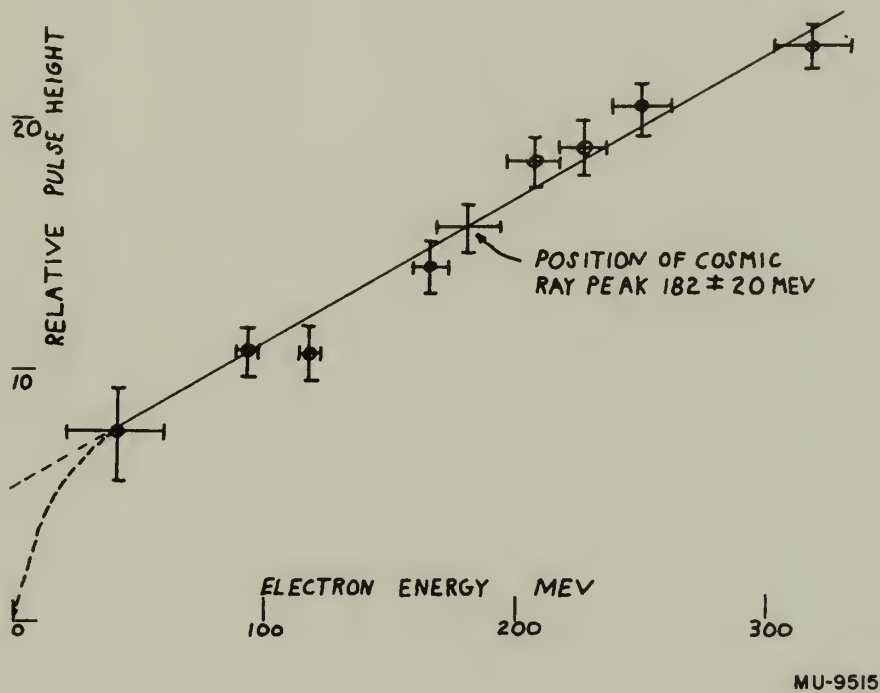


Fig. 16. Graph of the linear response of the spectrometer from 42 Mev to 319 Mev.



Fig. 1. Graph of the decay of the percentage of the original amount of the substance over time.

TABLE I  
GLASS CHARACTERISTICS

Composition	(by weight)
	PbO    52%
	SiO <sub>2</sub> 42%
	K <sub>2</sub> O    3%
	Na <sub>2</sub> O    3%
Size	12.25 inches in diameter
	7    inches in length (per cylinder)
Type	Corning Code 8392
Density	3.89 grams per cubic centimeter
Optical Characteristics	
	Index of refraction 1.649 for the sodium "D" line
	Dispersion value ( $\nu$ ) 33.8
	Light transmission (one cylinder) (5% accuracy)
	6707 A    80%
	5890 A    80%
	4916 A    80%
	4358 A    80%
	4046 A    10%
	4000 A    0%
	3650 A    0%
Shower Characteristics	
	Radiation length 2.81 cm
	Critical energy 18 Mev
	Average photon track length 200 to 500 Mev 2.6 cm (7)
	Ionization energy loss $\sim 1.36 \text{ Mev/cm}^2$
	Cherenkov radiation $\sim 954 \text{ ev/cm}$ (relativistic velocities)



## BIBLIOGRAPHY

- |                                      |  |
|--------------------------------------|--|
| 1. Hess                              | Physik. Z., Vol 13, p. 1084, 1912  |
| 2. Hess and Steinmaurer              | Physik. Z., Vol 27, p. 159, 1926   |
| 3. Lawrence, E. and<br>Edlefsen, N.  | Science Vol 72, p. 376, 1930   |
| 4. Kantz and Hofstadter              | Nucleonics, Vol 12, No. 3, pp. 36-43, 1954   |
| 5. Rossi, B.                         | High-Energy Particles, Prentice-Hall,<br>1952, Chapter V   |
| 6. Halliday, D.                      | Introductory Nuclear Physics, Wiley and<br>Sons, 1950, p. 439  |
| 7. Sternheimer, R.                   | AECU Report Nos. 2982, 2983, 2984  |
| 8. Heitler, W.                       | Quantum Theory of Radiation, 2nd Edition,<br>Oxford Univ., P. 241  |
| 9. Cherenkov, P.                     | Compt. rend. acad. sci. URSS, Vol 2,<br>p. 451, 1934   |
| 10. Frank and Tamm                   | Compt. rend. acad. sci. URSS, Vol 14,<br>p. 109, 1937  |
| 11. Marshall, J.                     | Annual review of Nuclear Science,<br>Stanford Reviews, 1954, p. 142  |
| 12. Kantz, A.                        | Electron Induced Showers, HEPL Report<br>No. 17, May 1954, Stanford Univ., p. 83                                     |
| 13. Bowman and Thomas                | Multichannel Pulse-height Analyzer,<br>University of California Radiation Labora-<br>tory Report No. UCRL-2164, 1953 |
| 14. Fermi, E.                        | Nuclear Physics, Univ. of Chicago Press,<br>1950, p. 221a  |
| 15. Winckler, J. and<br>Anderson, K. | Phys. Rev. Vol 93, p. 596, 1954  |
| 16. Janossy, L.                      | Cosmic Rays, Oxford, 1950, p. 397  |













28455

Thesis  
J478

Jester  
A total absorption  
spectrometer for gamma  
rays.

28455

Thesis  
J478

Jester  
A total absorption  
spectrometer for gamma rays.

thesJ478

A total absorption spectrometer for gamm



3 2768 002 10765 8

DUDLEY KNOX LIBRARY